An aggregate model of the positive electrode system of the lead/acid cell
II. Simulation results

R. R. Nilson and R. C. Chaplin
Department of Production Technology, Massey University, Private Bag, Palmerston North (New Zealand)

(Received July 13, 1992)

Abstract

An aggregate model has been developed to represent the positive electrode system of the lead/acid cell. This model represents all cell parts that influence the behaviour of the positive electrode. The aggregate model assumes three elemental models. Results are obtained by employing the four models together. The aggregate model has parameters determined from cell dimensions, the active material and the elemental models. Cell current is the independent variable; voltage, current, charge state and acid distributions throughout the electrode system are determined. The model is used to simulate a 100 A h traction cell for a standard 20 A discharge, a 0.5 h rest and a 20 A charge cycle and variations including a 3.5 A and 140 A discharge and several model parameter sensitivity runs. Comprehensive results are given and compared with experimental data. The findings compare very well and establish the model as valid tool for simulating the positive electrode system.

Introduction

The aggregate model is a new and specialized model that represents the detailed structure and mechanisms of the lead/acid cell operating under normal service conditions [1–3]. A comprehensive model of this nature has been lacking to date.

The network cylinders or channels that make up the model are designated m, μ, h, s, n and r-channels. These represent the positive active mass (AM) macrostructure, microstructure, homogeneous (inactive) structure, adjacent separator region, adjacent negative plate region and associated reservoir region, respectively. The electrical and transport properties of this network are taken to describe the behaviour of the real system.

This paper defines model parameters, including channel dimensions, based on a standard traction cell and experimental measurements for an adopted AM. It gives comprehensive results for a standard discharge/charge cycle and variations. The results obtained are discussed in the light of published experimental data and compared with additional experiments associated with the model development.

0378-7753/93/$6.00

Aggregate model parameters and functions

Model parameters

Model parameters were selected to match the cell used in associated experiments. This cell was a 100 A h traction cell (type N7) manufactured by Chloride Batteries New Zealand Limited.

A number of the parameters relate directly to the cell dimensions and are given in Table 1.

The remaining parameters relate to the AM structure. In the absence of detailed AM data for the N7 cell, published data for positive AM that had paste composition and formation conditions that most closely matched those for the N7 cell [4] were adopted. From this data, the equivalent gram μ-channel volume was taken as the equivalent gram microstructure pore volume. The latter has been defined elsewhere [2]. Subtraction of this volume from the total pore volume on the adopted accumulative pore volume curve defined the equivalent gram m-channel volume. This assumed the volume of the h-channel was negligible, which was consistent with the low cell cycle life. The division of microstructure and macrostructure volumes by this approach occurred at a radius of 0.35×10^{-6} m. Transferring this radius onto the adopted accumulated pore surface curve defined the equivalent gram μ-channel and m-channel surface areas. The average positive AM porosity was calculated from the adopted total pore and solid volume for a gram of fully charged AM. The final few parameters were taken from a second source of data [5]. The h-channel and n-channel tortuosity factors and n-channel porosity were taken directly from this data, while the μ-channel and m-channel tortuosity factors were assumed to be the average of unity and the value given in the data. The average value was used since the m-channel/μ-channel trunk/branch structure inherently models a highly tortuous system where the individual components themselves need not have a large tortuosity factor.

The aggregate model parameters described above are summarized in Table 2. The aggregate model dimensions derived from these parameters are given in Table 3.

TABLE 1

Some aggregate model parameters

Parameter description (symbol)	Value
Number of positive half plates (N_p)	6
Parameter description (symbol)	**Value ($\times 10^{-3}$ m)**
Plate height (H_p)	218
Plate width (W_p)	136
Half positive plate thickness (S_p)	2.55
Combined positive grid height (H_g)	21
Combined positive grid width (W_g)	17
Separator assembly thickness (S_s)	3.6
Half negative plate thickness (S_n)	2.05
Cell case width, inside (W_c)	152
Cell case thickness, inside (S_c)	62
Electrolyte solution height (H_{c0})	300

TABLE 2

Remaining aggregate model parameters

Parameter description (symbol)	Value
Average positive active mass porosity (ρ_p)	0.518[a]
Positive macrostructure	
Equivalent gram volume (10^{-6} m^3 g^{-1}) (V_m)	0.066[a]
Equivalent gram surface (m^2 g^{-1}) (S_m)	0.08[a]
Surface roughness (f_m)	1.2[b]
Tortuosity (θ_m)	1.3[c]
Positive microstructure	
Equivalent gram volume ($\times 10^{-6}$ m^3 g^{-1}) (V_μ)	0.050[a]
Equivalent gram surface (m^2 g^{-1}) (S_μ)	3.52[a]
Surface roughness (f_μ)	2.0[b]
Tortuosity (θ_μ)	1.3[c]
Nonparticipating positive active mass tortuosity (θ_h)	2.19[d]
Average negative mass active porosity (ρ_n)	0.548[d]
Negative active mass tortuosity (θ_n)	1.18[d]

[a]Ref. 4.
[b]Estimate from micrographs ref. 4.
[c]Discounted value ref. 5.
[d]Ref. 5.

TABLE 3

Aggregate model dimensions

(a) Model component	Length (m)	Cross section (m^2)
r-channel	5.18×10^{-2}	9.31×10^{-12}
n-channel	2.42×10^{-3}	2.53×10^{-11}
s-channel	3.60×10^{-3}	6.88×10^{-11}
h-channel	5.58×10^{-5}	1.29×10^{-11}
m-channel	3.28×10^{-3}	1.23×10^{-11}
μ-channel	2.83×10^{-6}	1.01×10^{-14}
(b) Component numbers		
μ-channels per m-channel		1.07×10^{6}
m-channels per equivalent gram		1.62×10^{6}
m-channels per cell		2.59×10^{9}

Model functions

Acid concentration dependent functions for the equilibrium potential of the PbO_2 electrode, the resistivity of H_2SO_4 solution, the diffusion coefficient of H_2SO_4 in solution, and the anodic and cathodic exchange current density of the PbO_2 electrode must be known to operate the model. The first three functions were fitted to polynomials in concentration using established experimental data [6, 7]. The exchange current density functions are far from certain. The approach taken here was to adopt particular

reaction orders and likely values for the rate constants [8] to define the functions and to incorporate a constant factor to allow adjustment of the rate constants.

Aggregate model results

Results for a standard case

Figures 1 to 8 present comprehensive model results for the standard case of a medium 20 A full discharge followed by a 0.5 h rest and 20 A charge. The solid, small-dash and large-dash line types are associated with the discharge, rest and charge portions of the discharge/charge cycle, respectively. A description of important features for this case, and typical of other cases, is given below.

Discharge capacity

The positive-plate voltage reached a value of ~1.450 V at the end of discharge in 4.0 h (Fig. 1). That is, the cell had a discharge capacity of 80 A h at the 4 h rate. This corresponds to an 89 A h capacity at the 5 h rate of 17.8 A (assuming typical derating curves [9]).

Initial discharge stage

The initial stage is marked by an instantaneous, then short but relatively rapid, drop in plate voltage. The instantaneous voltage drop is 0.022 V from the open-circuit value of 1.766 V. Change in concentration cannot occur instantaneously and therefore change in electrode equilibrium potential is not a factor here. Figure 6 shows that the contribution of the solution potential drop is between 0.001 and 0.010 V, and is dependent on the position in the plate. By elimination, this means that the remaining (and largest) portion of the instantaneous voltage is due to the electrode overpotential.

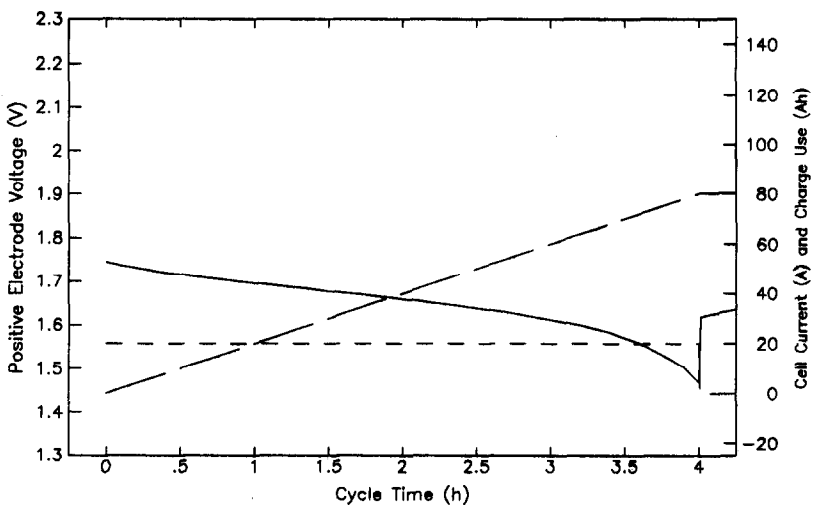

Fig. 1. Discharge voltage for 20 A full discharge: (solid) positive electrode voltage (V); (small dash) cell current (A), and (large dash) charge usage (A h). Results for 20 A discharge, 0.5 h rest and 20 A charge.

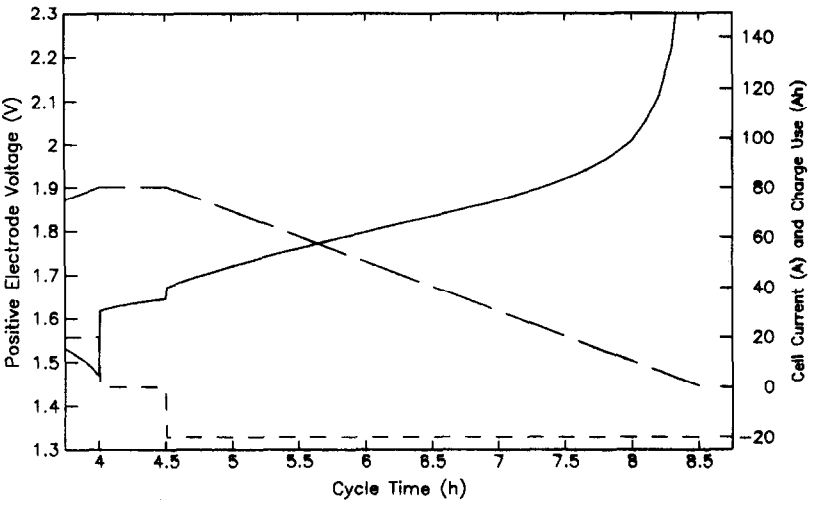

Fig. 2. Rest and charge voltage for 20 A full discharge: (solid) positive electrode voltage (V); (small dash) cell current (A), and (large dash) charge usage (A h). Results for 20 A discharge, 0.5 h rest and 20 A charge.

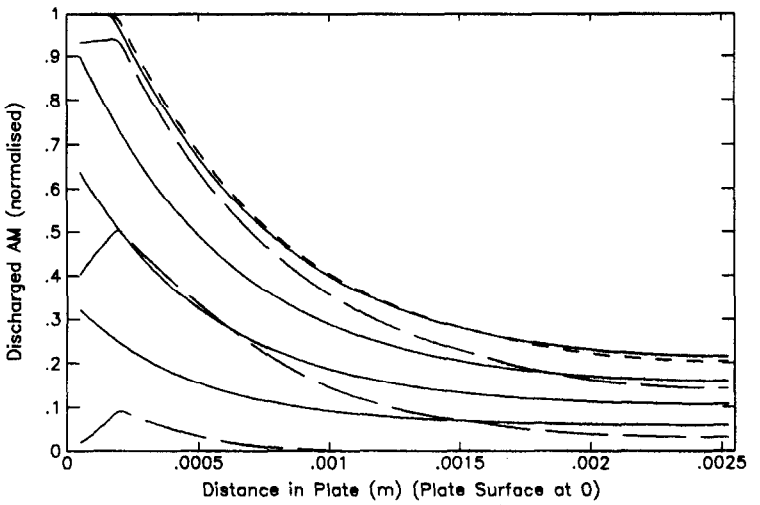

Fig. 3. Discharged plate active mass for 20 A full discharge: (solid) discharge profiles at 1.0, 2.0, 3.0 and 4.0 h bottom to top; (small dash) rest profile at 4.3 h, and (large dash) charge profiles at 5.0, 7.0 and 8.4 h top to bottom. Results for 20 A discharge, 0.5 h rest and 20 A charge, discharged active mass defined as: 1-(charge state).

Consider now the short, but relatively rapid, drop in plate voltage. Figure 6 indicates that the solution potential drop is essentially constant. Observations of the model in operation, however, show a relatively rapid drop in acid concentration in the plate. The electrode equilibrium potential decreases with decreasing acid concentration, and the electrode overpotential increases with decreasing acid concentration,

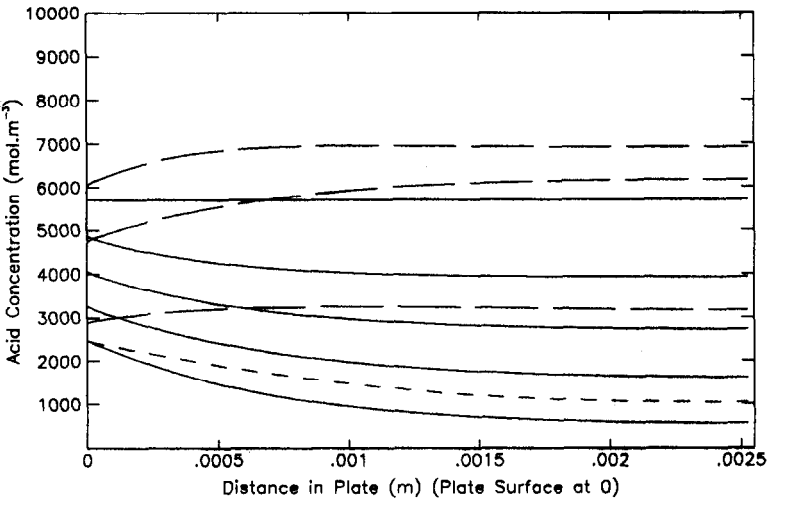

Fig. 4. Plate acid for 20 A full discharge: (solid) discharge profiles at 0.0, 1.0, 2.0, 3.0 and 4.0 h top to bottom; (small dash) rest profile at 4.3 h, and (large dash) charge profiles at 5.0, 7.0 and 8.4 h bottom to top. Results for 20 A discharge, 0.5 h rest and 20 A charge.

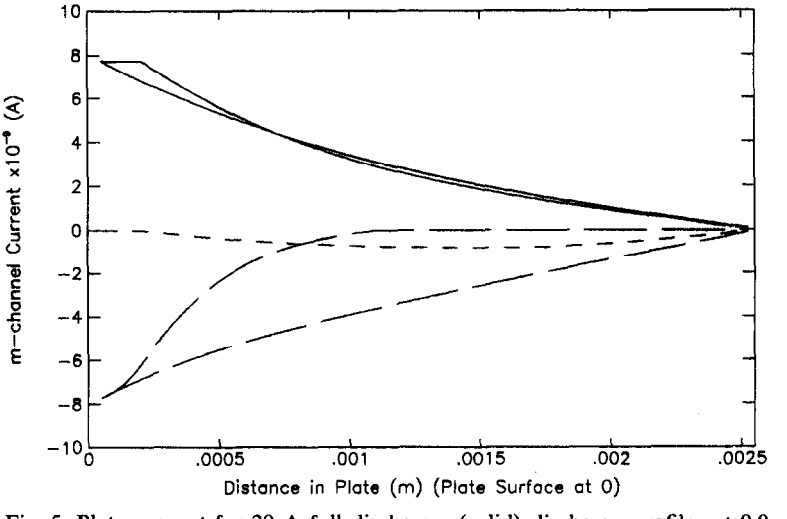

Fig. 5. Plate current for 20 A full discharge: (solid) discharge profiles at 0.0 and 4.0 h left and right; (small dash) rest profile at 4.3 h, and (large dash) charge profiles at 5.0 and 8.4 h right and left. Results for 20 A discharge, 0.5 h rest and 20 A charge.

because of the positive cathodic exchange current reaction order. Together, these effects account for the observed fall in plate voltage. The rapid decrease in concentration is not sustained as concentration gradients develop and acid is supplied to the plate from the separator.

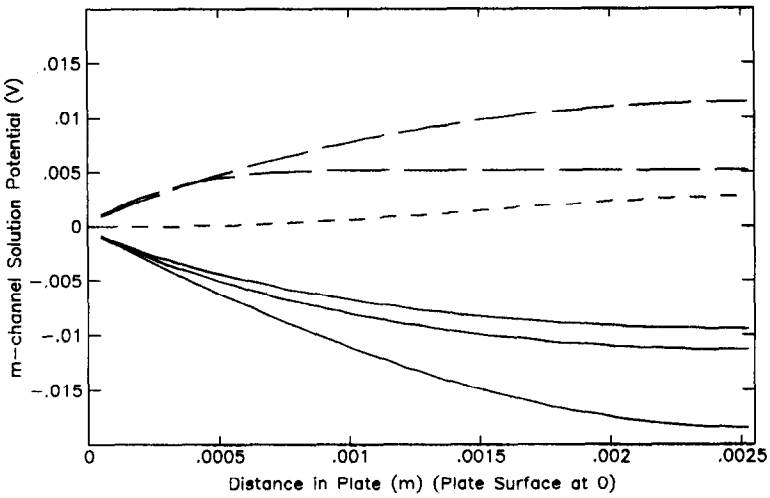

Fig. 6. Plate solution potential for 20 A full discharge: (solid) discharge profiles at 0.0, 2.0 and 4.0 h top to bottom; (small dash) rest profile at 4.3 h, and (large dash) charge profiles at 5.0 and 8.4 h top and bottom. Results for 20 A discharge, 0.5 h rest and 20 A charge.

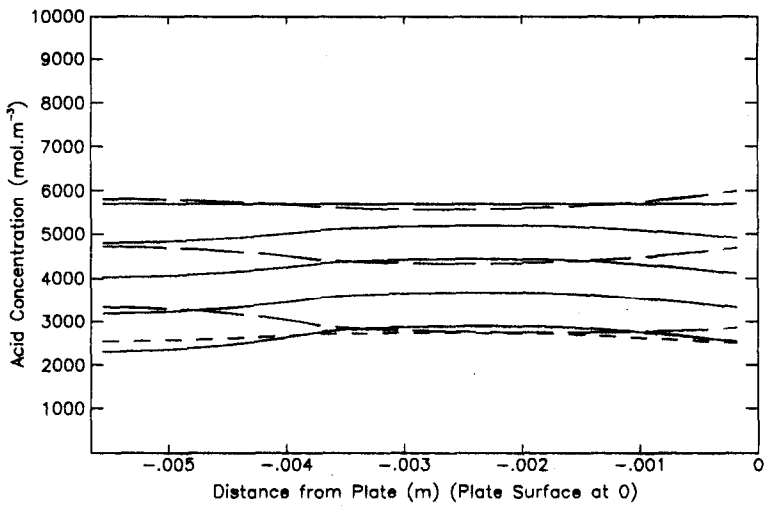

Fig. 7. Negative and separator acid for 20 A full discharge: (solid) discharge profiles at 0.0, 1.0, 2.0, 3.0 and 4.0 h top to bottom; (small dash) rest profile at 4.3 h, and (large dash) charge profiles at 5.0, 7.0 and 8.4 bottom to top. Results for 20 A discharge, 0.5 h rest and 20 A charge.

Intermediate discharge state

The majority of the discharge time is spent in the intermediate discharge stage. In this case, the plate voltage exhibits a gradual decline. Figure 6 shows that the potential drop due to solution resistance does not change significantly during this time. Reference to the internal acid concentration (Fig. 4) indicates that a decline in acid

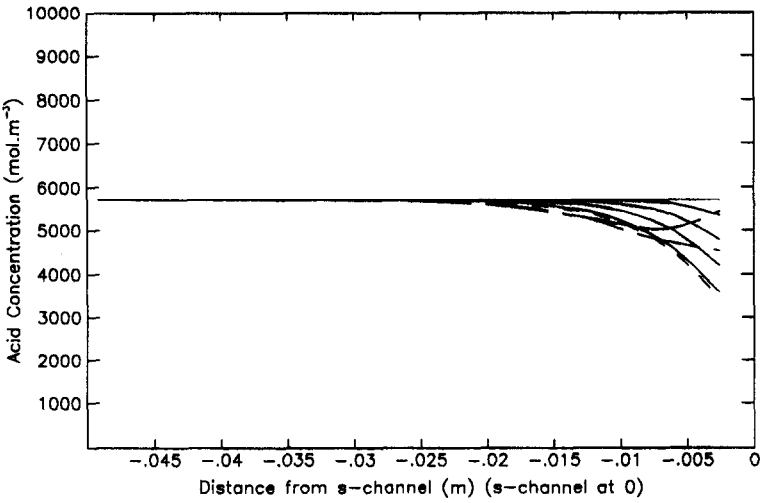

Fig. 8. Reservoir acid for 20 A full discharge: (solid) discharge profiles at 0.0, 1.0, 2.0, 3.0 and 4.0 h top to bottom; (small dash) rest profile at 4.3 h, and (large dash) charge profiles at 7.0 and 8.4 h bottom to top. Results for 20 A discharge, 0.5 h rest and 20 A charge.

concentration, and the effect that this has on the electrode equilibrium potential and overpotential, is the main mechanism for the voltage drop. In this case, however, the decline in acid concentration is somewhat slower than before. It can be seen form Figs. 4, 7 and 8 that the decline in acid concentration is an effect of restricted transport within the cell components.

Final discharge stage

In the final stage of the discharge, the plate voltage shows a rapid fall. Three factors contribute to this behaviour. First, the solution potential drop increases at this stage of the discharge. This is due, in part, to the increase in acid resistivity as the acid concentration approaches zero. It is also due to the effect of the progression of the reaction region into the plate interior. The progression can be seen by the moving fronts for the discharged plate AM and plate current in Figs. 3 and 5, respectively. This requires the discharge current to pass through an acid solution component of increasing length (and, therefore, resistance) before reaching the reaction region. The maximum drop in solution potential is approximately 0.02 V (Fig. 6).

Second, the effect of electrode equilibrium potential, discussed above, rapidly increases in magnitude as the acid concentration in the plate approaches zero. The drop in this potential in the last hour of the discharge is approximately 0.1 V (estimated from concentration in Fig. 4). This is of the same order as the total potential drop for the first 3 h of the discharge.

Third, the effect of the overpotential, as discussed above, rapidly increases in magnitude as the concentration approaches zero. By elimination, this must be greater than 0.100 V at the end of the discharge compared with 0.022 V or less at the beginning of the discharge.

Open-circuit rest stage

The rest stage is between discharge and charge when there is no net cell current (cell open-circuit). The voltage/time characteristic here is given in the early part of

Fig. 2. It shows an instantaneous, then gradual, rise in plate voltage. The instantaneous voltage rise is due to a reduction in solution potential drop (Fig. 6) and in electrode overpotential as the cell current is discontinued.

Consider now the gradual voltage rise. Figure 4 shows that the acid concentration within the plate gradually increases during the rest period as acid is supplied from outside the plate. This change in acid concentration dictates a gradual increase in equilibrium potential for the electrode that, in turn, accounts for the observed gradual rise in the voltage characteristic.

A discharge/charge reaction occurs internally within the plate during the rest stage. This reaction is driven by variations in equilibrium potential due to the nonuniform concentration distribution (Fig. 4). The latter is sustained by the supply of acid from the separator region. As a result, AM near the plate surface continues to discharge and is balanced by an equal charge of AM in the plate interior. The current distribution in Fig. 5, and the redistribution of AM during the rest stage in Fig. 3, are both evidence of this.

Initial charge stage

The initial stage is marked by an instantaneous, then relatively rapid, rise in plate voltage. The reasons for this are similar to those given for the initial stage of the discharge. Again, the relatively rapid rise in acid concentration is not sustained.

Intermediate charge stage

In the intermediate stage of the charge, the voltage displays a gradual increase. This is a continuation of the initially rapid effects seen at the beginning of the charge and is controlled by a gradual increase in acid concentration (Fig. 4). Again, it compares directly with the intermediate discharge stage. The one difference in the charge case is that the solution potential rise (compared with a fall in the discharge case) reduces with increasing acid concentration, since the solution resistivity reduces. This can be seen in Fig. 5.

Final charge stage

The final stage of the charge shows a rapid rise in plate voltage. There is not a large increase in acid concentration at this stage (Fig. 4). This means that the electrode equilibrium potential and the solution potential rise do not contribute in a major way to the rapid increase in voltage. By elimination, this leaves the electrode overpotential as the main contributor. The high overpotential is to be expected since the current density increases rapidly as the charge current is concentrated onto a vanishing reaction surface area (the effective PbO_2 surface).

Other model results

Simulations were performed for slow and fast discharge rates, AM with increased tortuosity, AM with a significant proportion of nonparticipating AM, and AM with an increased exchange current. In all cases, the discharge is followed by a 0.5 h rest and a 20 A charge.

Results for a 3.5 A slow discharge

A high discharge capacity of 134 A h was obtained in this case because of two effects. First, more time is available for acid to diffuse into the plates from elsewhere and as a result the plate acid concentration decreases slowly. This gives a higher electrode equilibrium potential and a lower overpotential than in the standard case.

Second, the lower current here gives a lower exchange current and therefore a lower overpotential than in the standard case.

The discharge voltage/time characteristic showed the dominant role of the electrode equilibrium potentials. For example, at the 30 h mark, the plate acid concentration corresponded to an equilibrium potential of 1.645 V. This is very near the plate voltage of 1.630 V. It is only at the end of the discharge when the acid concentration is very low that the electrode overpotential was significant.

The rest stage involved only a small amount of AM redistribution because of the small concentration and corresponding equilibrium potential gradients involved in the slow discharge.

The voltage at the beginning of the charge was lower than in the standard case because of a lower plate acid concentration at this time. Later in the charge, the plate acid concentration became very high as the large amount of acid produced was, to some extent, contained in the plate. As a result, the plate voltage towards the end of charge was higher than that for the standard case, given the same amount of charge restored.

Model results for a 140 A fast discharge

A cell capacity of 28 A h was obtained in this case. Typical derating curves based on the 5 h capacity from the standard case predict a capacity of 38 A h. At full discharge, the lowest plate acid concentration was 2337 mol m^{-3}. This is not a particularly low value and shows that neither the electrode equilibrium potential nor the solution resistance contribute in a major way to the full discharge voltage. This means the rather low capacity was due to a high overpotential that is sensitive to the rather uncertain exchange current density. When the simulation was repeated with the cathodic exchange current increased by a factor of 10^2, the cell capacity was 49 A h.

The discharge voltage/time characteristic had the same general features as in the standard case. The AM distribution showed an abrupt boundary between discharged and charged AM.

During the rest stage there was a considerable rearrangement of AM due to the large concentration and corresponding equilibrium potential gradients near the surface of the plate. The charge voltage/time characteristic showed a significant rise part way through the charge due to a rapid loss in charge surface area as a large portion of AM became fully charged.

Model results with m and μ-channel tortuousity 1.7 standard

The discharge capacity of 64.2 A h was considerably less than that of the standard case due to a more rapid drop in plate acid concentration in the plate interior. This has the usual adverse effects on electrode equilibrium potential and overpotential. The drop in acid concentration is to be expected with the increased acid transport difficulties of the more tortuous structure.

In other respects, the observed characteristics are similar to those of the standard case.

Model results with 20% nonparticipating active mass

A low capacity of 56.6 A h was obtained in this case due to a concentration gradient in the nonparticipating AM reducing the acid concentration at the reacting region. The reduced concentration gives the usual low electrode equilibrium potential and a high overpotential. The high overpotential conditions were compounded by a

reduced AM reaction area. In addition, the nonparticipating AM solution resistance increased the solution potential drop.

In other respects, the characteristics are similar to those for the standard case.

Model results with exchange currents standard ×10

A capacity of 87.0 A h was obtained on this case due to a smaller overpotential with increased exchange current. It was only at the end of the discharge and at the end of the charge that the overpotential contributions were large.

The AM distribution showed that the high cathodic exchange current gives a more distinct division between the discharge and charged AM than is seen in the standard case.

Discussion

Aggregate model dimensions

The model cross-sectional areas correspond to characteristic radii of 1.98×10^{-6} and 0.0568×10^{-6} m for the m and μ-channel, respectively. When pores of these dimensions are superimposed on micrographs of the adopted AM, the m-channel sizes were typical of large voids between crystallite agglomerates and the μ-channel sizes were typical of large voids within the agglomerate structure and very small voids between agglomerates. In both cases, the dimensions are close to those observed but biased slightly towards the larger voids. This bias can also be seen in the division of microstructure and macrostructure. Determined visually from the micrographs, the dividing radius was set at 0.20×10^{-6} m. By equating discharge volume changes to void volumes in the microstructure, the model sets the dividing radius at 0.35×10^{-6} m. This suggests a slight shift in the definition of the μ-channel volume to include small pores between agglomerates in addition to the voids within the agglomerates.

Cell capacity

The model parameters were set for a cell having a nominal capacity of 100 A h at the 5 h rate. In the standard case the model gave a very similar capacity of 89 A h at this rate.

Using the model results for the slow, medium and fast discharge cases, the fit of the predicted cell capacity to Peukert's equation gave a power term in the range 1.25 to 1.30. This was self-consistent and close to expected values [10].

Discharge voltage/time curve

The discharge voltage/time curve has the normal form of a slow decline that increases rapidly near the end of the discharge. The macrohomogeneous model does not predict such a rapid decline at the end of the discharge [11].

One particular set of published experimental data was selected for comparison with the model results [12]. The selected data were for an electric vehicle cell similar to that modelled, involved direct measurements of the positive plate voltage as calculated by the model and used discharge and charge rates close to that modelled.

Figure 9 gives the discharge results for the model and the selected data. The discharge capacity has been normalized to 100 A h and the open-circuit voltage, which is a function of initial acid concentration, made equal.

It can be seen that the model results agree closely with the experimental results.

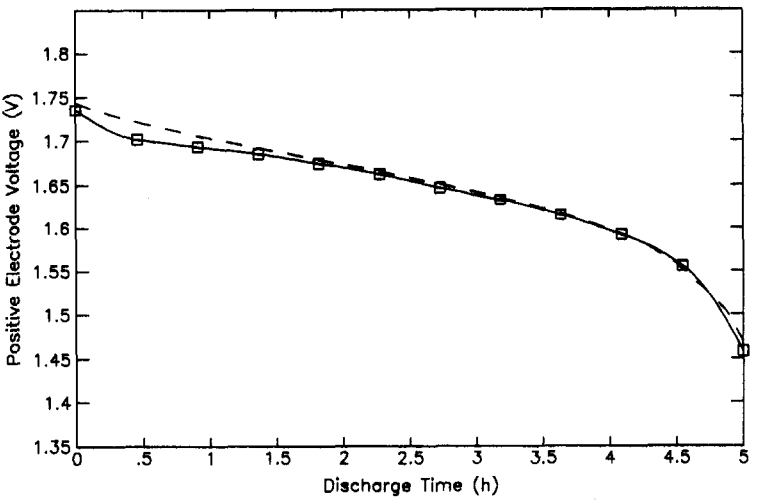

Fig. 9. Experimental and model discharge voltage: (□/solid) experimental results (ref. 12); (small dash) model results for standard discharge case (20 A full discharge, 0.5 h rest and 20 A charge). Capacity scaled to 100 A h, 5 h discharge.

Charge voltage-time curve

The charge voltage-time curve has the normal form of a slow rise which rapidly increases near the end of charge. Nevertheless, two features are missing. First, a voltage peak at the beginning of charge is sometimes observed [13]. This may be due to PbO_2 encapsulation during deep discharge, an effect noted but not accounted for in the charge surface area model [2]. Second, the increasing potential at the end of charge normally levels out. This occurs when the charge current is diverted into the gassing reaction. The aggregate model does not account for the gassing reaction.

Figure 10 gives the charge results of the model, together with the selected data introduced above. It can be seen that the model results give reasonable agreement with the selected data. In addition to the features already noted, variation at the beginning of the charge is likely to be exaggerated by different acid concentration distributions. This is because the selected data is for an undetermined rest time and associated acid redistribution.

Internal active mass distribution

The model predicts a sharply defined boundary between the discharged and charged AM at high discharge currents, and a more graded boundary at medium and low discharge currents. This is in good agreement with experimental observations [11, 14].

The model results for the 140 A discharge are compared with published experimental data for a similar discharge current density [11] in Fig. 11. There is close agreement between the model and experimental results. The macrohomogeneous model gave a more graded boundary at high discharge rates [11].

Role of acid transportation

The transport of acid has been seen to be the key factor in limiting the cell capacity. This is consistent with recent studies of cells with different AM [4] and confirms the adoption of macropore/micropore model structure.

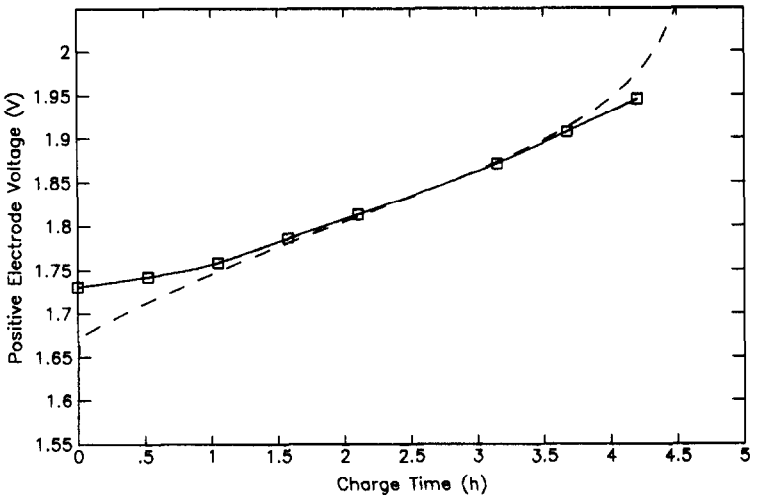

Fig. 10. Experimental and model charge voltage: (□/solid) experimental results (ref. 12); (small dash) model results for standard charge case (20 A full discharge, 0.5 h rest and 20 A charge). Capacity scaled to 100 A h, 5 h rate.

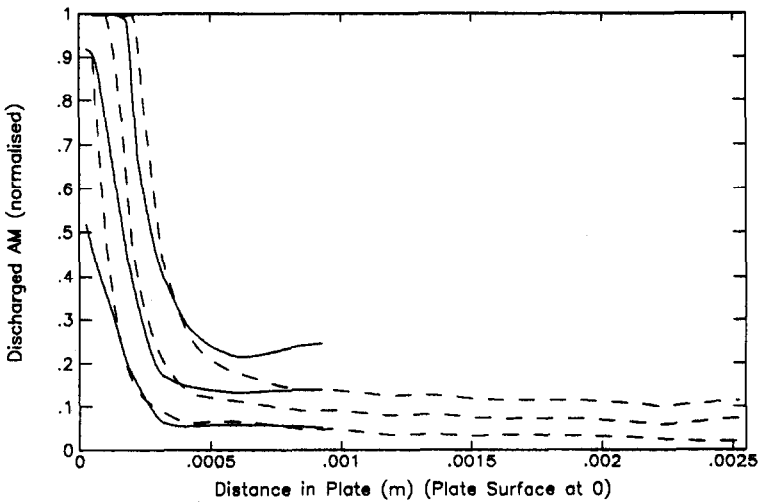

Fig. 11. Experimental and model discharged plate active mass: (solid) experimental profiles at 25, 50 and 100% (ref. 11), full discharge capacity bottom to top; (small dash) model profiles at 28.5, 57.1 and 85.7%, full discharge capacity bottom to top. Discharge current density approximately 1000 A m^{-2}.

Effects of cycling

The model was operated with increasing quantities of nonparticipating AM and gave a steady decrease in cell capacity. Experimental results reveal a wide variation in effects. Most commonly, after the initial few discharge/charge cycles where the

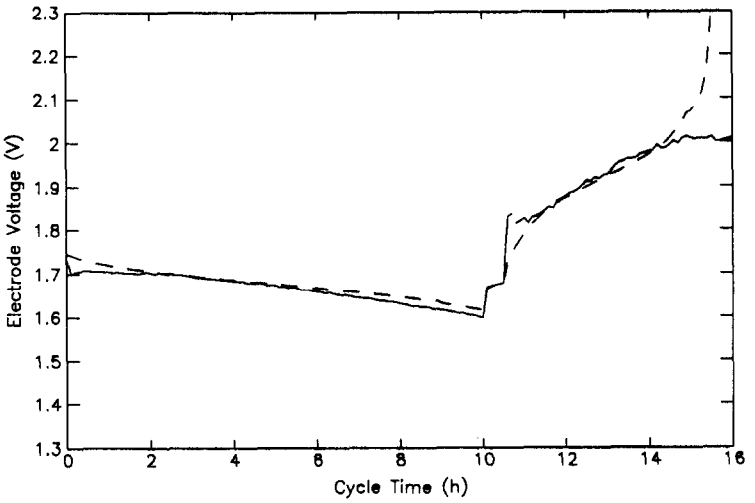

Fig. 12. Model and commercial cell 10 A discharge electrode voltage: (solid) experimental results, and (dash) model results. Cycle: 100 A h/10 A discharge, 0.5 h rest and 20 A charge.

capacity may increase, there is a gradual decreasing in capacity [15]. The initial increase in capacity is, in effect, the completion of unfinished plate formation.

Voltage/time characteristics and the N7 cell experiments

A large number of experiments were performed on the N7 cell. In these experiments, discharge rate and depth were varied and cell terminal voltage, cell current, reservoir PbO_2 reference electrode to cell positive voltage, reservoir acid concentration and cell gassing were measured. Cell temperature was kept at 25 °C by a temperature-controlled water jacket. For the discharge, rest and start of charge, the positive electrode voltage was estimated from the cell voltage, a resistive term for post-grid and separator resistance and the negative plate equilibrium potential given the concentration measurement. For the remainder of the charge, when the negative plate overpotential becomes significant, an alternative procedure was used. This estimated the positive electrode voltage from the reference electrode voltage, a resistive term half that of before and positive electrode equilibrium potential given the concentration measurement.

Model simulations were performed to correspond to the N7 cell experiments. In these simulations, the model parameters were estimated for the N7 cell as described for the standard case, the diffusion coefficient in the reservoir increased ($\times 40$) to attempt to account for stirring due to gassing and concentration gradients, and the cathodic exchange current adjusted ($\times 0.44$) to give a model capacity the same as the N7 cell.

The model and experimental results showed the same form subject to the qualifications already given for the published experimental results above. The range tested was for discharge depths of 10 to 100 A h and discharge rates of 5 to 40 A. Generally, the numerical agreement was within 30 mV at low and medium currents, and 60 mV at high currents. An example 100 A h/10 A discharge is given in Fig. 12.

The model can be seen to simulate closely the N7 cell. Discrepancies of the magnitude observed are expected given the uncertainties associated with model pa-

rameters and the experimental voltage estimation procedures, all of which increase with current.

Conclusions

The aggregate model has successfully simulated the positive electrode system of the lead/acid cell. It has produced results in good agreement with experimental studies.

The model has a unique contribution in representing the positive electrode system in that it: (i) accounts for AM microstructure and macrostructure; (ii) accounts for nonparticipating AM; (iii) defines capacity and surface area of the AM; (iv) accounts for acid transport in all cell components; (v) applies to the discharge, rest and charge situations; (vi) applies over a wide range of practical currents, and (vii) defines variable distributions within the AM.

References

1 R. R. Nilson, *J. Power Sources, 43* (1993) 1–12.
2 R. R. Nilson, *J. Power Sources, 43* (1993) 25–37.
3 R. R. Nilson and R. I. Chaplin, *J. Power Sources, 43* (1993) 13–23.
4 D. Pavlov and R. Bastavelova, *J. Electrochem. Soc., 133* (1986) 241.
5 K. Micka, M. Svatá and V. Koudelka, *J. Power Sources, 4* (1979) 43.
6 H. Bode, *Lead-Acid Batteries,* Wiley–Interscience, New York, 1977.
7 K. Micka and I. Rousar, *Electrochim. Acta, 18* (1973) 629.
8 N. A. Hampson, P. C. Jones and R. F. Phillips, *Can. J. Chem., 46* (1986) 1325.
9 D. I. Linden, *Handbook of Batteries and Fuel Cells,* McGraw-Hill, New York, 1984.
10 M. Asher, N. A. Hampson, S. Kelly and G. S. Holmes, *Surf. Tech., 11* (1980) 17.
11 D. Simonsson, *J. Appl. Electrochem., 3* (1973) 151.
12 W. G. Sunu and B. W. Burrows, *J. Electrochem. Soc., 128* (1981) 1405.
13 P. Ekdunge and D. Simonsson, *J. Electrochem. Soc., 132* (1985) 252.
14 T. G. Chang, *J. Electrochem. Soc., 131* (1984) 1755.
15 K. V. Kordesch (ed.), *Batteries,* Vol. 2, *Lead-Acid Batteries and Electric Vehicles,* Marcel Dekker, New York, 1977.